Journal of Testing and Evaluation, **Vol. 38, No. 2**
Paper ID JTE101907
Available online at: www.astm.org

Application of artificial neural network for fatigue life prediction under interspersed mode-I spike overload

J. R. Mohanty[a*], B. B. Verma[a], P. K. Ray[b], D. R. K Parhi[b]

[a] *Department of Metallurgical and Materials Engineering*

[b] *Department of Mechanical Engineering*

National Institute of Technology, Rourkela 769008, India

Abstract

The objective of this study is to design multi-layer perceptron artificial neural network (ANN) architecture in order to predict the fatigue life along with different retardation parameters under constant amplitude loading interspersed with mode-I overload. Fatigue crack growth tests were conducted on two aluminum alloys 7020-T7 and 2024-T3 at various overload ratios using single edge notch tension specimens. The experimental data sets were used to train the proposed ANN model to predict the output for new input data sets (not included in the training sets). The model results were compared with experimental data and also with Wheeler's model. It was observed that the model slightly over-predicts the fatigue life with maximum error of + 4.0 % under the tested loading conditions

Keywords: Artificial neural network; Overload ratio; Multi-layer perceptron; Retardation parameters.

***** Corresponding author. Tel.: +91 661 2464553 (J. R. Mohanty)
Email address: guddy95@yahoomail.co.in, guddy95@gmail.com,

Nomenclature

a	crack length measured from edge of the specimen (mm)
a_{i}	crack length corresponding to the 'i^{th}' step (mm)
a_{j}	crack length corresponding to the 'j^{th}' step (mm)
a_{ol}	crack length at overload (mm)
a_{d}	retarded crack length (mm)
$a_{\mathrm{d}}^{\mathrm{A}}$	retarded (ANN) crack length (mm)
$a_{\mathrm{d}}^{\mathrm{E}}$	retarded (experimental) crack length (mm)
$a_{\mathrm{d}}^{\mathrm{W}}$	retarded (Wheeler) crack length (mm)
B	plate thickness (mm)
C	constant in the Paris equation
COD	crack opening displacement
'cgr'	crack growth rate
$\left(C_{\mathrm{p}}\right)_{\mathrm{i}}$	retardation parameter
$\mathrm{d}a/\mathrm{d}N$	crack growth rate (mm/cycle)
$(\mathrm{d}a/\mathrm{d}N)_{\mathrm{retarded}}$	retarded crack growth rate (mm/cycle)
E	modulus of elasticity (MPa)
E_{rr}	sum-squared error
$\mathrm{f}(g)$	geometrical factor
$\mathrm{f}(.)$	activation function
F	remotely applied load (N)
K	stress intensity factor ($\mathrm{MPa}\sqrt{m}$)
K_{IC}	plane strain fracture toughness ($\mathrm{MPa}\sqrt{m}$)
$K_{\max}$	maximum stress intensity factor ($\mathrm{MPa}\sqrt{m}$)
$K_{\max}^{\mathrm{B}}$	maximum (base line) stress intensity factor ($\mathrm{MPa}\sqrt{m}$)
K_{ol}	stress intensity factor at overload ($\mathrm{MPa}\sqrt{m}$)
ΔK	stress intensity factor range ($\mathrm{MPa}\sqrt{m}$)

'lay'	layer number
'msif'	maximum stress intensity factor
n	exponent in the Paris equation
N	number of cycles or fatigue life
N_{d}	number of delay cycle
$N_{\mathrm{d}}^{\mathrm{A}}$	number of delay cycle (ANN)
$N_{\mathrm{d}}^{\mathrm{E}}$	number of delay cycle (experimental)
$N_{\mathrm{d}}^{\mathrm{W}}$	number of delay cycle (Wheeler)
$N_{\mathrm{f}}^{\mathrm{A}}$	final number of cycles (ANN)
$N_{\mathrm{f}}^{\mathrm{E}}$	final number of cycles (experimental)
'olr'	overload ratio
p	shaping exponent in the Wheeler model
r	label for r^{th} neuron in hidden layer 'lay-1'
r_{pi}	current plastic zone size corresponding to the 'i^{th}' cycle (mm)
r_{po}	overload plastic zone size (mm)
R_{ol}	overload load ratio
s	label for s^{th} neuron in the hidden layer 'lay'
'sifr'	stress intensity factor range
t	iteration number
w	plate width (mm)
$W_{\mathrm{sr}}^{\{\mathrm{lay}\}}$	weight of the connection from neuron r in layer 'lay-1' to neuron s in layer 'lay'
y_1, y_2, y_3	inputs to the ANN
γ	retardation correction factor
λ	plastic zone correction factor
ν	Poison's ratio
α	momentum coefficient
η	learning rate
$\delta_{\mathrm{s}}^{\{\mathrm{lay}\}}$	local error gradient

σ_{ys} yield point stress (MPa)

σ_{ut} ultimate stress (MPa)

Introduction

Most load bearing structural components are subjected to random loading in service consisting of distinguished peaks. These load cycle interactions can have a very significant effect on the fatigue crack propagation which is a path dependent process [1]. A tensile overload can retard or even arrest the growing fatigue crack while a compressive under load can accelerate it [2-8]. Overload-induced retardation has a significant effect on fatigue crack growth as it enhances the life of the structure. A number of mechanisms may be responsible to explain the crack retardation phenomena, including plasticity induced crack-closure, blunting and / or bifurcation of the crack-tip, residual stresses and strains, strain-hardening, crack-face roughness, oxidation of crack faces etc [5, 9-15]. However, for design purposes it is particularly difficult to generate a universal algorithm to quantify these sequence effects on fatigue crack growth, due to the number and to the complexity of the mechanisms involved in this problem [16]. Irrespective of significant ambiguity and disagreements as regards to the exact mechanism of retardation, a number of empirical models [17] have been proposed. But, a technological gap still exists in the automatic prediction of fatigue life in case of mode-I spike load. This can be accomplished by the use of ANN (artificial neural network).

ANN is a new class of computational intelligence system, useful to handle various complex problems with a capacity to learn by examples. The first ANN concept was adopted by McCulloch and Pits [18] in 1943, who suggested the cell model. Although some pioneer work was undertaken in 1949 [19] by focusing attention on the learning system of human brain, but the actual development on ANN concept started towards 1980 through various studies [20]. It has emerged as a new field of soft-computing to deal with many multivariate complex problems for which an accurate analytical model does not exist [21-23]. ANN has proved to be a powerful and versatile computational tool in the application of a number of engineering fields [24-29]. In recent years, ANN has been also introduced in the field of fatigue in order to predict fatigue life [30-36]. A brief review on the topic has been presented by Jia et al. [37]. They used ANN to predict

valuable fatigue responses in order to facilitate the development of design guidelines for hybrid material bonded interfaces.

In this study, ANN has been used to predict fatigue crack growth rate (FCGR) under mode-I spike load with various overload ratio (R_{ol}). The simulated results of unknown load ratio (not included in the training set) have been utilized to calculate the retardation parameters (a_d and N_d) as well as the residual life. The predicted results have been compared with the experimental data conducted on 7020-T7 and 2024-T3 Al-alloys. It is observed that the results are in good agreement with the experimental findings.

2. Experimental procedure

The fatigue tests were performed on 7020-T7 and 2024-T3 aluminum alloys using single-edge notched (SEN) tension specimens having a thickness of 6.5mm. The chemical composition and the mechanical properties of the alloys are given in Table 1 and 2 respectively. The specimens were made in the longitudinal transverse (LT) direction from the plate.

All the experiments were conducted in ambient temperature on a servo-hydraulic dynamic testing machine (*Instron*-8502) with 250 kN load cell, interfaced to a computer. The test specimens were fatigue pre-cracked under mode-I loading to an *a/w* ratio of 0.3 and were subjected to constant load amplitude test (i.e. progressive increase in ΔK with crack extension) maintaining a load ratio of 0.1. The sinusoidal loads were applied at a frequency of 6 Hz. The crack growth was monitored with the help of a COD gauge mounted on the face of the machined notch. The stress intensity factor K was calculated using equations proposed by Brown and Srawley [38] as follows;

$$K = \mathrm{f}(g).\frac{F\sqrt{\pi a}}{wB} \tag{1}$$

where, $\mathrm{f}(g) = 1.12 - 0.231(a/w) + 10.55(a/w)^2 - 21.72(a/w)^3 + 30.39(a/w)^4$ (2)

The fatigue crack growth test was continued up to an *a/w* ratio of 0.4 and then a mode-I spike (static) overload was applied. After the application of overload, the pre-overload fatigue crack growth test (i.e. constant amplitude loading at load ratio of 1.0) was continued till the specimen fractured. The overloading was done at a loading rate of 8.0 kN/min at different overload ratios such as 2.0, 2.25, 2.35, 2.5, 2.6, and 2.75 for six 7020

T7 Al-alloy specimens and 1.5, 1.75, 2.0, 2.1, 2.25 and 2.5 for six 2024 T3 Al-alloy specimens. The overload ratio is defined as

$$R_{\mathrm{ol}} = \frac{K_{ol}}{K^{\mathrm{B}}_{\mathrm{max}}} \tag{3}$$

where, $K^{\mathrm{B}}_{\mathrm{max}}$ is the maximum stress intensity factor for base line test.

3. Artificial Neural Network

3.1 Fundamental approach

The term “neural network” refers to a collection of neurons, their connections and the connection strengths between them. The knowledge is acquired during the training process by correcting the corresponding weights so as to minimize an error function. There are three types of learning in ANN technology: supervised, unsupervised and reinforcement. In case of supervised learning (learning with a teacher), the network is trained by optimizing corresponding weights in such a way that the significant outputs can be obtained for the inputs not belonging to the training set. The unsupervised training is based on organizing the structure so that similar stimuli activate similar neurons where there is no pre-defined output and the network finds differences and affinities between the inputs. The reinforcement learning, which is a particular form of supervised training attempts to learn input-output vectors by trial and error through maximizing a performance function (named reinforcement signal).

Back propagation networks are in fact the powerful networks which refer to a multi-layered, feed-forward perceptron trained with an error-back propagation algorithm (error minimization technique). The architecture of a simple back propagation ANN is a collection of nodes distributed over a layer of input neurons, one or more layers of hidden neurons and a layer of output neurons. Neurons in each layer are interconnected to subsequent layer neurons with links, each of which carries a weight that describes the strength of that connection. Various non-linear activation functions, such as sigmoidal, tanh or radial (Gaussian) are used to model the neuron activity. Inputs are propagated forward through each layer of the network to emerge as outputs. The errors between those outputs and the target (desired output) are then propagated backward through the network and then connection weights are adjusted so as to minimize the error.

3.2 Design and analysis of ANN model for crack growth rate prediction

The neural network used in the present investigation is a multi-layer feed forward perceptron [23] trained with the standard back propagation algorithm [39]. It consists of one input layer, one output layer and seven hidden layers. Hence, the total numbers of layers in the network are nine. The chosen numbers of layers have been selected empirically so as to facilitate training. The three input parameters associated with the input layer are as follows;

Stress intensity factor range = "sifr"; Maximum stress intensity factor = "msif"; Overload ratio = "olr".

The output layer consists of one output parameter (i.e. crack growth rate = "cgr"). The neurons associated with the input and output layers are three and one respectively. The neurons in seven hidden layers are twelve, twenty four, hundred, thirty five, and eight respectively. The neurons are taken in order to give the neural network a diamond shape as shown in Fig. 1. The neural network has been written in the C^{++} programming language and all the training tests have been performed on a personal computer in MATLAB environment. During training and during validation, the input patterns fed to the neural network comprise the following components:

$y_1^{\{1\}}$ = stress intensity factor range (4)

$y_2^{\{1\}}$ = maximum stress intensity factor (5)

$y_3^{\{1\}}$ = overload ratio (6)

These input values are distributed to the hidden neurons which generate outputs given by [23]:

$$y_s^{\{\text{lay}\}} = \text{f}\left(v_s^{\{\text{lay}\}}\right) \quad (7)$$

where, $$v_s^{\{\text{lay}\}} = \sum_r W_{sr}^{\{\text{lay}\}} . y_r^{\{\text{lay}-1\}} \quad (8)$$

'lay' = layer number (2 to 8)

s = label for s^{th} neuron in the hidden layer 'lay'

r = label for r^{th} neuron in hidden layer 'lay-1'

$W_{sr}^{\{\text{lay}\}}$ = weight of the connection from neuron r in layer 'lay-1' to neuron s in layer 'lay'

f *(.)* = activation function, chosen in this work as the hyperbolic tangent function:

$$\mathrm{f}(x) = \frac{e^{\mathrm{x}} - e^{-\mathrm{x}}}{e^{\mathrm{x}} + e^{-\mathrm{x}}} \tag{9}$$

During training, the network output θ_{actual}, may differ from the desired output θ_{desired} as specified in the training pattern presented to the network. A measure of the performance of the network is the instantaneous sum-squared difference between θ_{desired} and θ_{actual} for the set of presented training patterns:

$$E_{\text{rr}} = \frac{1}{2} \sum_{\substack{all \\ training \\ patterns}} \left(\theta_{\text{desired}} - \theta_{\text{actual}}\right)^2 \tag{10}$$

Where θ_{actual} represents crack growth rate ("cgr")

The error back- propagation method is employed to obtain the network [23]. This method requires the computation of local error gradients in order to determine appropriate weight corrections to reduce 'E_{rr}'. For the output layer, the error gradient $\delta^{\{9\}}$ is:

$$\delta^{\{9\}} = \mathrm{f}'\left(V_1^9\right)\left(\theta_{\text{desired}} - \theta_{\text{actual}}\right) \tag{11}$$

The local gradient for neurons in hidden layer {lay} is given by:

$$\delta_{\text{s}}^{\{\text{lay}\}} = \mathrm{f}'\left(V_{\text{s}}^{\{\text{lay}\}}\right)\left(\sum_k \delta_{\text{k}}^{\{\text{lay}+1\}} W_{\text{ks}}^{\{\text{lay}+1\}}\right) \tag{12}$$

The synaptic weights are updated according to the following expressions:

$$W_{\text{sr}}\left(t+1\right) = W_{\text{sr}}\left(t\right) + \Delta W_{\text{sr}}\left(t+1\right) \tag{13}$$

and $$\Delta W_{\text{sr}}\left(t+1\right) = \alpha \Delta W_{\text{sr}}\left(t\right) + \eta \delta_{\text{s}}^{\{\text{lay}\}} y_{\text{r}}^{\{\text{lay}-1\}} \tag{14}$$

where,

α = momentum coefficient (chosen empirically as 0.2 in this work)

η = learning rate (chosen empirically as 0.35 in this work)

t = iteration number, each iteration consisting of the presentation of a training pattern and correction of the weights.

The final output from the neural network is:

$$\theta_{\text{actual}} = f\left(V_1^{\{9\}}\right) \tag{15}$$

where,

$$V_1^{\{9\}} = \sum_r W_{1\text{r}}^{\{9\}} y_{\text{r}}^{\{8\}} \tag{16}$$

3.3 Application of neural network architecture

Proper selection of input and output parameters and their normalization are the two primary objectives to design a suitable ANN architecture. The proposed ANN model has been developed using back propagation architecture with three inputs and one output. The two crack driving forces: stress intensity factor range (ΔK) and maximum stress intensity factor (K_{max}) have been chosen as the two inputs. The selection of ΔK and K_{max} as two inputs for the present model is based on the principle of Unified Approach [5]. According to this principle, fatigue is considered as two-parametric problem because there are two driving forces (ΔK and K_{max}) required to obtain fatigue crack growth. The third input is the overload ratio (R_{ol}) as the amount of retardation varies with the overload ratio. Crack growth rate ($\mathrm{d}a/\mathrm{d}N$) has been selected as the output for the present study. As far as normalization of input and output parameters are concerned, classical normalization, where the range is scaled between 0 and 1, may not be applicable in every ANN model. To make the input amenable for successful learning to minimize the overall sum-squared error, the two input parameters ΔK and K_{max} have been normalized between 1 and 4, while the other one, overload ratio (R_{ol}) has been normalized between 1 and 3. Similarly the output $\left(\frac{\mathrm{d}a}{\mathrm{d}N}\right)$ has been normalized between 0 and 3 for network training and testing. The inputs and outputs of the training sets (TS) have been constituted from $50 \times 50 \times 50$ experimental values of ΔK, K_{max} and $\left(\frac{\mathrm{d}a}{\mathrm{d}N}\right)$ data respectively for each of the overload ratios (i.e. R_{ol} = 2.0, 2.25, 2.5, 2.6, and 2.75 in case of 7020-T7 Al alloy and R_{ol} = 1.5, 1.75, 2.0, 2.25 and 2.5 in case of 2024-T3 Al alloy) separately for both the materials which has been kept ready to be fed to the trained ANN. The performance of the trained ANN model has been presented in Table 3. Figures 2 and 3 illustrate the mean square error (MSE) curves during the training of the model.

4. Results

4.1 Analysis of experimental results

The experimental values of crack length versus number of cycles for various overload ratios (R_{ol}) have been plotted in Figs. 4 and 5 respectively along with base line

data in case of both the materials. The crack growth rate, $\left(\frac{\mathrm{d}a}{\mathrm{d}N}\right)$ has been calculated by incremental polynomial method as per ASTM E647 [42]. The results have been plotted against stress intensity factor (ΔK) in Figs. 6 and 7 for the post overload portion covering both the regimes II and III of fatigue crack growth rate curve.

4.2 Analysis of ANN model results

The adopted multi-layer perceptron (MLP) neural network model has been applied to simulate the crack growth rate of an unknown set of overload ratio (R_{ol} = 2.35 for Al 7020-T7 and R_{ol} = 2.1 for Al 2024-T3) as validation set (VS). The performance of the trained ANN model has been presented in Table 3. The input parameters i.e. stress intensity factor range (ΔK), maximum stress intensity factor (K_{max}) and overload ratio for the validation set have been fed to the trained ANN model in order to predict the corresponding crack growth rate $\left(\frac{\mathrm{d}a}{\mathrm{d}N}\right)$ which was not included during training. The predicted results have been presented in Figs. 8 and 9 respectively along with experimental data for comparison. It is observed that the simulated da/dN-ΔK points follow the experimental ones quite well. The number of cycles has been calculated from the simulated $\left(\frac{\mathrm{d}a}{\mathrm{d}N}\right)$ values by taking the experimental 'a' and 'N' values of the overload point as the initial values and assuming an incremental crack length of 0.05mm in steps. The predicted a-N value of the ANN model has been compared with the experimental data in Figs. 10 and 11 respectively for both the materials. The a-da/dN and N-da/dN curves have been given in Figs. 12 to 15.

4.3 Comparison with 'Wheeler Model'

For determination of the various retardation parameters such as retarded crack length (a_d) and delay cycles (N_d), it is necessary to calculate the shaping exponent in Wheeler model. The Wheeler retardation relation for the delay in crack growth due to a single tensile overload is given by:

$$\left(\frac{\mathrm{d}a}{\mathrm{d}N}\right)_{\text{retarded}} = \left(C_{\mathrm{p}}\right)_{\mathrm{i}}\left[C(\Delta K)^{\mathrm{n}}\right] \tag{17}$$

where, C and n are Paris constants whose values have been determined from the experimental data and presented in Table 4. The Wheeler's retardation parameter $(C_{\mathrm{p}})_{\mathrm{i}}$ is given by the following equation:

$$\left(C_{\mathrm{p}}\right)_{\mathrm{i}} = \left(\frac{r_{\mathrm{pi}}}{[a_{\mathrm{ol}} + r_{\mathrm{po}} - a_{\mathrm{i}}]}\right)^{\mathrm{p}} \tag{18}$$

where, p = empirically determined shaping parameter

a_{ol} = crack length at overload

and r_{po} = overload plastic zone size, that can be calculated, assuming plane stress loading using the following expression:

$$r_{\mathrm{po}} = \frac{1}{\pi}\left(\frac{K_{ol}}{\sigma_{\mathrm{ys}}}\right)^2 \tag{19}$$

Assuming plane stress loading conditions, the current cyclic plastic zone r_{pi} can be calculated from the expression given below:

$$r_{\mathrm{pi}} = \frac{1}{\pi}\left(\frac{\Delta K}{2\sigma_{\mathrm{ys}}}\right)^2 \tag{20}$$

The presence of a net compressive residual stress field around the crack-tip reduces the usual size of the plane stress cyclic plastic zone size. Therefore, Ray et al. [43] introduced a plastic zone correction factor λ in the expression of the instantaneous cyclic plane stress plastic zone size in a compressive stress field.

$$r_{\mathrm{pi}} = \lambda\left(\frac{1}{\pi}\right)\left(\frac{\Delta K}{2\sigma_{\mathrm{ys}}}\right)^2 \tag{21}$$

Also from eqn.(17)

$$C_{p_i} = \frac{(da/dN)_{retard}}{C(\Delta K)^n} = \frac{(da/dN)_{retard}}{(da/dN)_{a=a_0}} \tag{22}$$

Equation (18) is now written as

$$\left(C_{\mathrm{p}}\right)_{\mathrm{i}} = \left(\frac{\lambda r_{\mathrm{pi}}}{[a_{\mathrm{ol}} + r_{\mathrm{po}} - a_{\mathrm{i}}]}\right)^{\mathrm{p}} = \gamma\left[\frac{r_{\mathrm{pi}}}{\left(a_{\mathrm{ol}} + r_{\mathrm{po}} - a_{\mathrm{i}}\right)}\right]^{\mathrm{p}} \tag{23}$$

where, γ is a correction factor which is expressed as $\gamma = \lambda^{p}$.

The values of γ , λ and p calculated using equations (22) and (23) are presented in Table 4 for both the materials. Using these values, the crack lengths and the corresponding number of cycles have been calculated. The resulting a-N curves are presented in Figs. 16 and 17 while da/dN-ΔK curves are presented in Figs. 18 and 19 along with experimental data and present ANN model of the post overload portion (up to the point where retardation ceases) for comparison. The different calculated retardation parameters have been given in Table 5 for the quantitative comparison of the predicted results.

5. Discussion and Conclusion

It is observed from the results (Table-5) that the error range of retarded crack length (a_d) predicted from the ANN model is -6 to -9 % whereas, it is +3 to +13 % in case of Wheeler model. Similarly, the error range of delay cycle (N_d) predicted from ANN model is +7 to +9 % whereas, it is -2 to -9 % in case of Wheeler model. It shows that the prediction accuracy of ANN model is better as far as the retardation parameters are concerned. Analyzing the end life of post overload period of the specimen, it is observed that the error range of fatigue life (N_f) is +1 to +4 % for both the alloys. From the above results it is evident that the proposed multi-layer perceptron ANN over-predicts the life with reasonable accuracy in comparison to experimental findings.

From the present investigation, it can be concluded that the proposed ANN model has proved to be an excellent computational tool for the prediction of residual fatigue life as well as the retardation parameters (a_d and N_d) in case of mode-I spike load. The predicted results are in good agreement with the experimental findings and also with the conventional Wheeler's model. It has been further verified that taking the single crack driving force (ΔK) instead of two crack driving forces (ΔK and K_{max}) along with overload ratio (R_{ol}) as inputs resulted poor prediction in crack growth rate (da/dN), thereby supporting the principle of Unified Approach. Therefore, it should be noted that proper selection of input and output parameters greatly affects the accuracy of the simulated results.

One of the shortcomings of the present ANN model is that it takes more computational time for proper training of the network to meet the target. Further, it has

the weakness of extrapolating model's predictions outside the training set region. The present form of the neural network architecture could provide better prediction results if the training data base could be enhanced by more experimental data. The use of other types of neural networks such as recurrent, associative memory, and self-organizing networks could also improve the prediction accuracy.

Acknowledgement

The authors wish to record their thanks to CSIR, India for sponsoring this project (project No. 22(373)/04/EMR II). They also thank Hindalco, Renukoot, India for supplying the Aluminium alloy for this research project.

References

[1] Sih, G.C., and Moyer, E.T., "Path depended nature of fatigue crack growth," Int. J. Eng. Fract. Mech., vol. 7, 1983, pp. 269-280.

[2] Paris, P.C., Tada, H., and Donald, J.K., "Service load fatigue damage—a historical Perspective," Int. J. Fatigue, vol. 21, 1999, pp. S35–S46.

[3] Skorupa, M., "Load interaction effects during fatigue crack growth under variable amplitude loading—a literature review, part 1: Empirical trends," Fatigue Fract. Eng. Mater. Struct., vol. 21, 1998, pp. 987–1006.

[4] Skorupa, M., "Load interaction effects during fatigue crack growth under variable amplitude loading—a literature review, part 2: Qualitative interpretation," Fatigue Fract. Eng. Mater. Struct., vol. 22, 1999 pp. 905–926.

[5] Sadananda, K., Vasudevan, A.K., Holtz, R.L., and Lee, E.U., "Analysis of overload effects and related phenomena," Int. J. Fatigue, vol. 21, 1999, pp. S233–S246.

[6] Lang, M., and Marci, G., "The influence of single and multiple overloads on fatigue crack propagation," Fatigue Fract. Eng. Mater. Struct., vol. 22, 1999, pp. 257–271.

[7] Suresh, S., "Fatigue of materials," 2nd ed. Cambridge, UK: Cambridge University Press, 1998.

[8] Broek, D., "The practical use of fracture mechanics," Dordrecht, The Netherlands: Kluwer Academic Publishers, 1988.

[9] Ramos, M.S., Pereira, M.V., Darwish, F.A., Motta, S.H., and Carneiro, M.A.,

"Effect of Single and Multiple Overloading on the Residual Fatigue Life of a Structural Steel," Fatigue Fract. Eng. Mater. Struct, vol. 26, 2003 pp. 115-121.

[10] Robin, C., Busch, M.L., Chergui, M., Lieurade, H.P., and Pluvinage, G., "Influence of Series of Tensile and Compressive Overloads on 316L Crack Growth," Fatigue Crack Growth Under Variable Amplitude Loading(ed J Petit D I Davidson, S Suresh and P Rabbe), Elsevier Applied Science, London, 1988, pp. 87-97.

[11] Ling, M.R., Schijve, J., "The Effect of Intermediate Heat Treatments on Overload Induced Retardation during Fatigue Crack Growth in an Al Alloy," Fatigue Fract. Eng. Mater. Struct., vol. 15, 1992 pp. 421-430.

[12] Suresh, S., "Micro Mechanisms of Fatigue Crack Growth Retardation Following Overloads," Eng. Fract. Mech., vol. 18, 1983, pp. 577-593.

[13] Elber, W., "The Significance of Fatigue Crack Closure," ASTM STP, vol. 486, 1971, pp. 230-242.

[14] Ohrloff, N., Gysler, A., and Lutjering, G., "Fatigue Crack Propagation Behaviour under Variable Amplitude Loading," in Fatigue Crack Growth Under Variable Amplitude Loading (ed by J Petit, D I Davidson, S Suresh and P Rabbe), Elsevier Applied Science, London, 1988, pp. 24-34.

[15] Meggiolaro, M.A., and de Castro, J.T.P., "On the dominant role of crack closure on fatigue crack growth modeling," Int. J. Fatigue, vol. 25, 2003, pp. 843-854.

[16] Murthy, A.R.C., Palani, G.S., and Iyer, N.R., "State-of-the-art review on fatigue crack growth analysis under variable amplitude loading," J. Institution of Engineers (India) IE-CV, vol. 85, 2004, pp. 118-129.

[17] McCulloch, W.S., and Pitts, W.A., "A logical calculus of the ideas immanent in nervous Activity," Bull. Math. Biophysics, vol. 943, No. 5, 1943, pp. 115-133.

[18] Hebb, D., "The Organisation of Behaviour," Willey, New York, USA, 1949.

[19] Hopfeld, J.J., "Neural Networks and Physical Systems with Emergent Collective Computational Abilities," Proc. Natl. Acad. Sci., vol. 79, 1982, pp. 2554-2558.

[20] Skapura, D., "Building neural networks," New York: ACM Press Addison-Wesley Publishing Company, 1996.

[21] Schalkoff, R.J., "Artificial neural networks," McGraw-Hill. NY 1997.

[22] Haykin, S., "Neural networks: a comprehensive foundation," New York:

Macmillan, 1994.

[23] Herzallah, R., and Al-Assaf, Y., "Control of non-linear and time-variant dynamic systems using neural networks," In: Proceedings of the 4th World Multiconference on Systemics, Cybernetics and Informatics, Florida, 2000.

[24] Mansoor, W., Al-Nashash, H. and Al-Assaf, Y., "Image classification using wavelets and neural networks," In: The 18th IASTED International Conference on Applied Informatics, Innsbruck, Austria, 2000.

[25] Al-Nashash, H., Al-Assaf, Y., Lvov, B., and Mansoor, W., "Laser speckle for materials classification utilizing wavelets and neural networks image processing techniques," J. Mater. Evaluat., vol. 59, 2001, pp. 1072–1078.

[26] Lee, C.S., Hwang, W., Park, H.C., and Han, K.S., "Failure of carbon/epoxy composite tubes under combined axial and torsional loading—1. Experimental results and prediction of biaxial strength by the use of neural networks," Comp. Sci. Techno., vol. 59, 1999, pp. 1779–1788.

[27] Aymerich, F., and Serra, M., "Prediction of fatigue strength of composite laminates by means of neural networks," Key. Eng. Mater. Vol. 144, 1998, pp. 231-240.

[28] Lee, J.A., Almond, D.P., and Harris, B., "The use of neural networks for the prediction of fatigue lives of composite materials," Comp. Part A: Appl. Sci. Manufact. Vol. 30, 1999, pp. 1159-1169.

[29] Meyer, S., Diegel, E., Bru¨ckner-Foit, A., and Mo¨slang, A., "Crack interaction modeling," Fatigue Fract. Eng. Mater. Struct. Vol. 23, 2000, pp. 315–323.

[30] Artymiak, P., Bukowski, L., Feliks, J., Narberhaus, S., and Zenner, H., "Determination of S-N curves with the application of artificial neural networks," Fatigue Fract. Eng. Mater. Struct. Vol. 22, 1999, pp. 723–728.

[31] Pleune, T.T., and Chopra, O.K., "Using artificial neural networks to predict the fatigue life of carbon and low-alloy steels," Nucl. Eng. Design, vol. 197, 2000, pp. 1–12.

[32] Venkatesh, V., and Rack, H.J., "A neural network approach to elevated temperature creep- fatigue life prediction," Int. J. Fatigue, vol. 21, 1999, pp. 225–234.

[33] Haque, M.E., and Sudhakar, K.V., "Prediction of corrosion-fatigue behavior of DP steel through artificial neural network," Int. J. Fatigue, vol. 23, 2001, pp. 1-4.

[34] Cheng, Y., Huang, W.L., and Zhou, C.Y., "Artificial neural network technology for the data processing of on-line corrosion fatigue crack growth monitoring," Int. J. Pres. Ves. Pip. Vol. 76, 1999, pp. 113–116.

[35] Pidaparti, R.M.V., and Palakal, M.J., "Neural Network Approach to Fatigue- Crack-Growth Predictions under Aircraft Spectrum Loadings," J. Aircraft, vol. 32, No. 4, 1995, pp. 825-831.

[36] Jia, J., and Davalos, J.F., "An artificial neural network for the fatigue study of bonded FRP- wood interfaces," Comp. Structures, vol. 74, 2006, pp. 106-114.

[37] **Brown**, W.F., **Srawley**, J.E. (1966) "Plane strain crack toughness testing of high strength metallic materials"**.** ASTM STP 410, ASTM, West Conshohocken, PA

[38] Werbos, P. J., "Backpropagation and neurocontrol: a review and prospectus," Int. Joint Conf. Neural Netw., vol. 1, 1989, pp. 209.

[39] Dinda, S., and Kujawski, D., "Corelation and prediction of fatigue crack growth for different R-ratios using K_{max} and ΔK^{+} parameters," Eng. Fract. Mech.vol. 71, No. 12, 2004, pp. 1779-1790.

[40] Noroozi, A.H., Glinka, G., and Lambert, S., "A two parameter driving force for fatigue crack growth analysis," Int. J. Fatigue, vol. 27, 2005, 1277-1296.

[41] ASTM Standard E647-05, 2007, "Standard test method for measurement of fatigue crack growth rates," *Annual Book of ASTM Standards*, vol 3, ASTM International, West Conshohocken, PA.

[42] Ray, P.K., Ray, P.K., and Verma, B.B., "A study on spot heating induced fatigue crack growth retardation" Fatigue Fract. Eng. Mater. Struct. Vol. 28, 2005, pp. 579-585.

List of Tables:

List of Figures:

Fig. 18 - Comparison of Wheeler, predicted (ANN) and experimental crack growth rate (7020-T7)

Fig. 19 - Comparison of Wheeler, predicted (ANN) and experimental crack growth rate (2024-T3)

Table-1 (Chemical composition)

Materials	Al	Cu	Mg	Mn	Fe	Si	Zn	Cr	Others
7020-T7	93.13	0.05	1.2	0.43	0.37	0.22	4.6	-	-
2024-T3	92.78	3.9	1.5	0.32	0.5	0.5	0.25	0.1	0.15

Table-2 Mechanical properties

Material	Tensile strength (σ_{ut}) MPa	Yield strength (σ_{ys}) MPa	Young's modulus (E) MPa	Poisson's ratio (ν)	Plane Strain Fracture toughness (K_{IC}) $MPa\sqrt{m}$	Elongation
7020-T7	352	315	70,000	0.33	50.12	21.54 % in 40 mm
2024-T3	469	324	73,100	0.33	37.0	19 % in 12.7 mm

Table 3 – Performance of ANN model during training

Material	Momentum Coefficient	Learning rate	Hidden neurons	MSE	Training epochs	Computational Time (Min.)
7020-T7	0.2	0.35	179	1.056×10^{-6}	6.861×10^{5}	727
2024-T3	0.2	0.35	179	1.034×10^{-6}	6.559×10^{5}	694

Table-4 Values of material parameters used in Wheeler model for the tested specimens

Material	C	n	λ	p	γ
7020-T7	6×10^{-8}	3.14763	3.5931	0.4246	1.7213
2024-T3	6×10^{-8}	3.2700	0.7385	0.3748	0.8926

Table 5 – Comparison of ANN and Wheeler model results with experimental data

Material	a_d^A mm	a_d^W mm	a_d^E mm	% error in a_d^A	% Error in a_d^W	N_d^A K cy.	N_d^W K cy.	N_d^E K cy.	% error in N_d^A	% error in N_d^W	N_f^A K cy.	N_f^E K cy.	% error in N_f^A
7020-T7	1.998	2.200	2.134	-6.373	+3.093	32.673	29.802	30.509	+7.093	-2.317	83.721	80.815	+3.596
2024-T3	1.990	2.450	2.181	-8.757	+12.333	40.716	34.518	37.599	+8.290	-8.194	139.384	136.804	+1.886

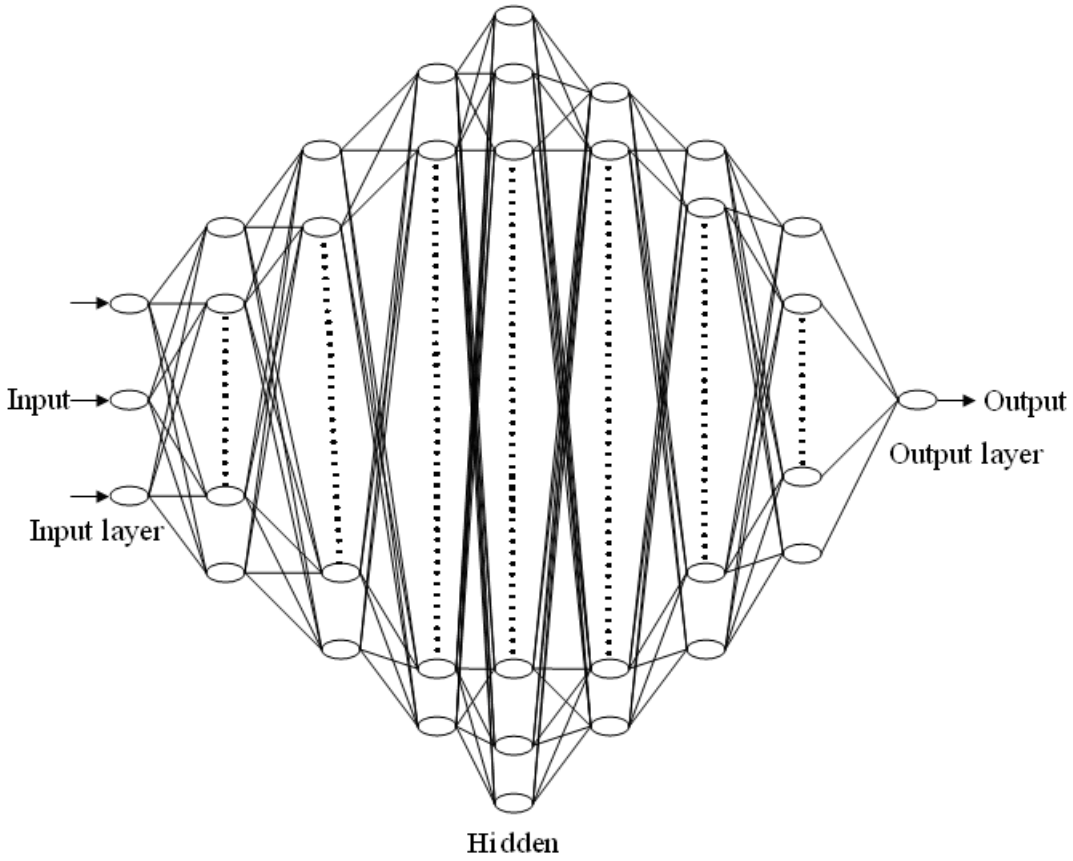

Fig. 1 - ANN architecture

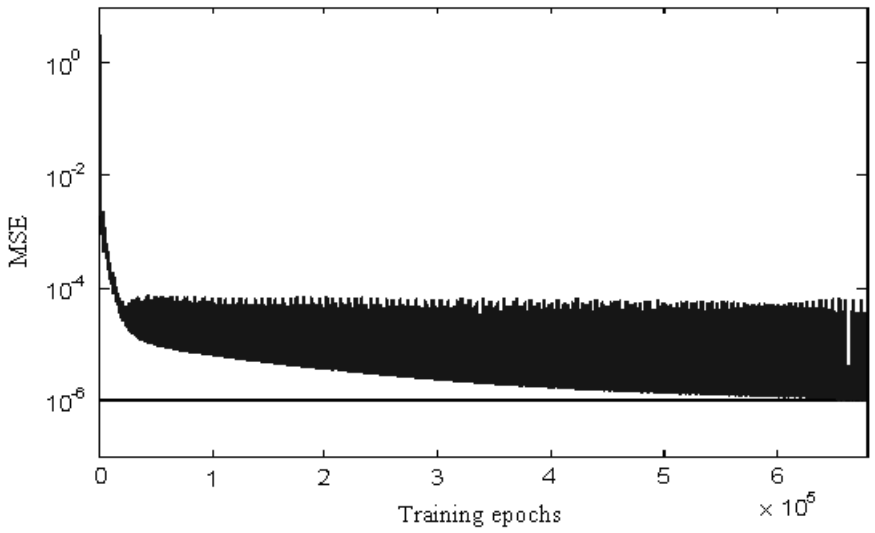

Fig. 2 – MSE curve obtained during training of ANN (Al 7020-T7)

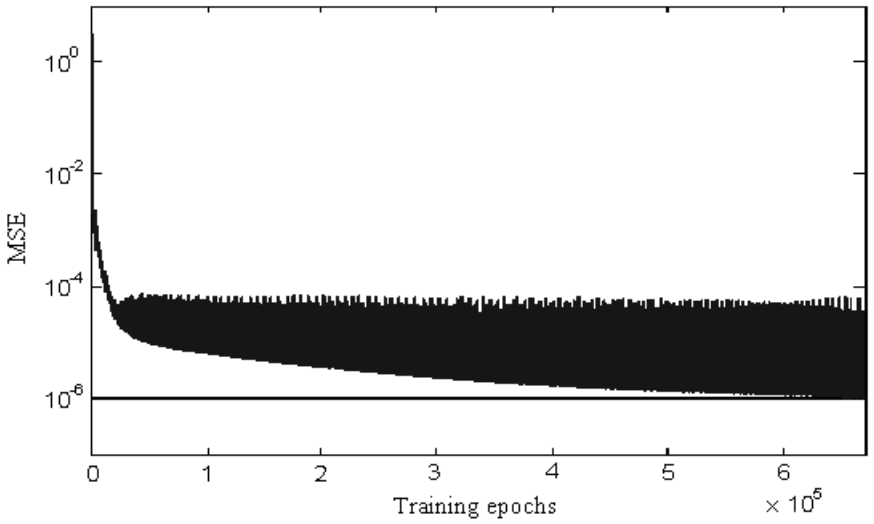

Fig. 3 – MSE curve obtained during training of ANN (Al 2024-T3)

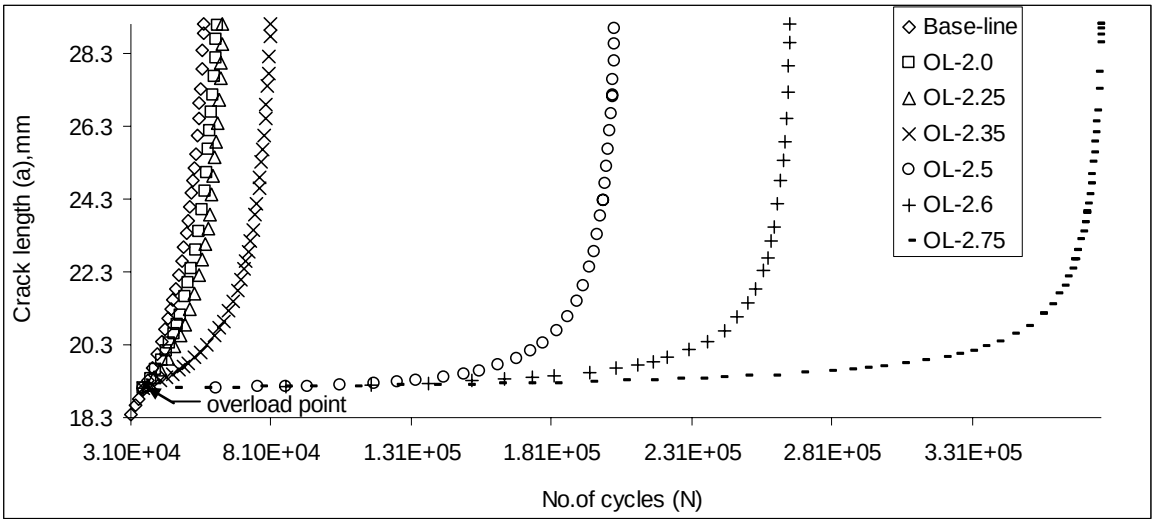

Fig. 4 - *a-N* curves for different overload ratios (7020-T7)

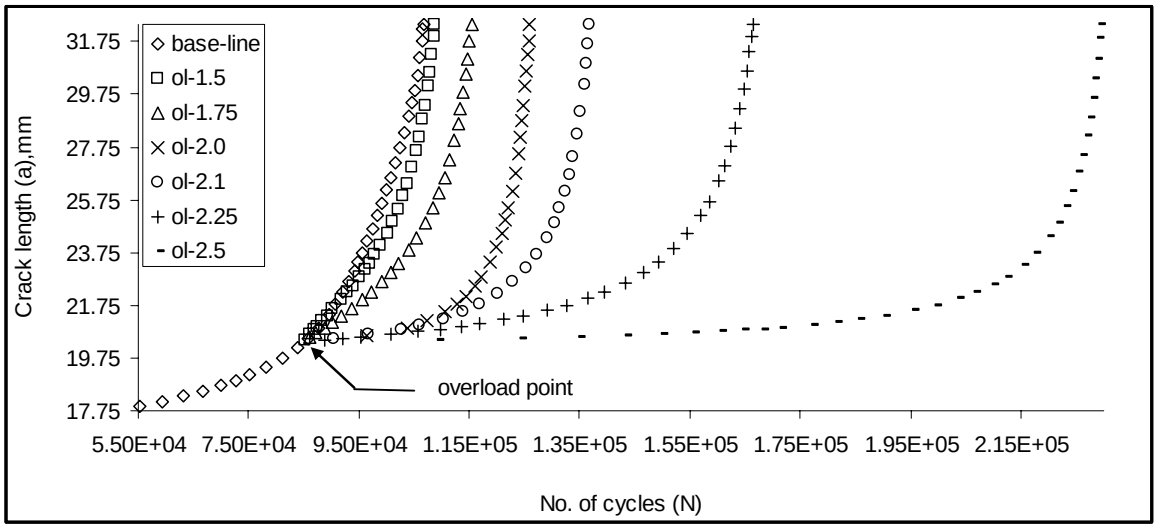

Fig. 5 - *a-N* curves for different overload ratios (2024-T3)

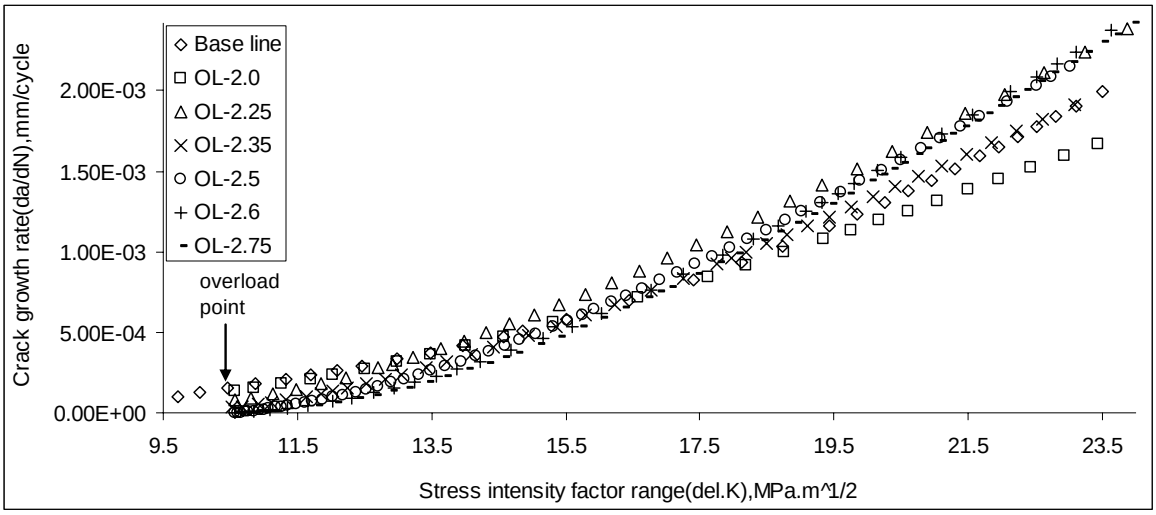

Fig. 6 -Variation of crack growth rate with stress intensity factor range (7020-T7)

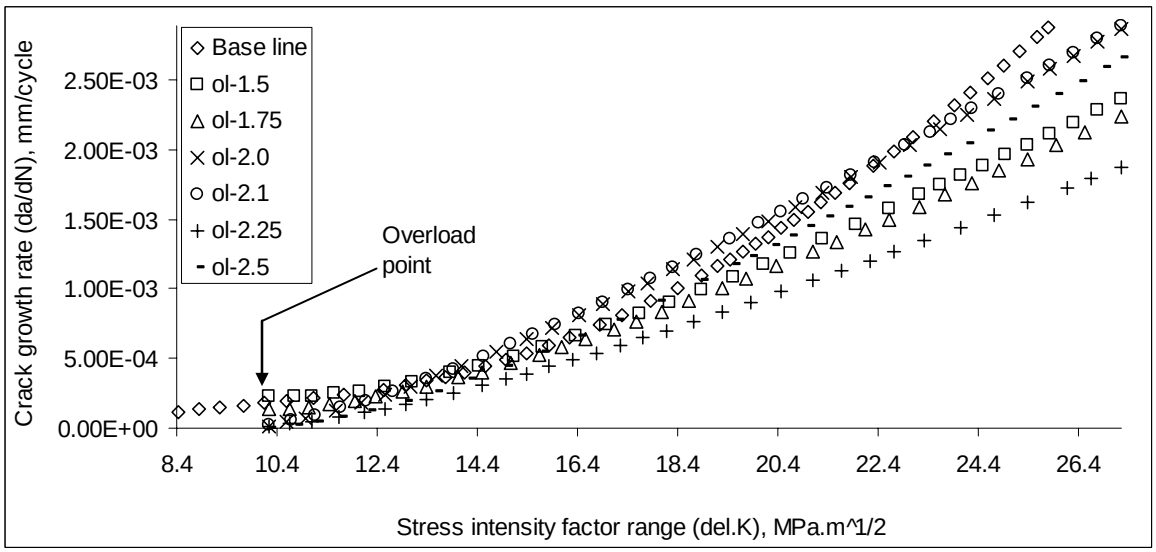

Fig. 7 -Variation of crack growth rate with stress intensity factor range (2024-T3)

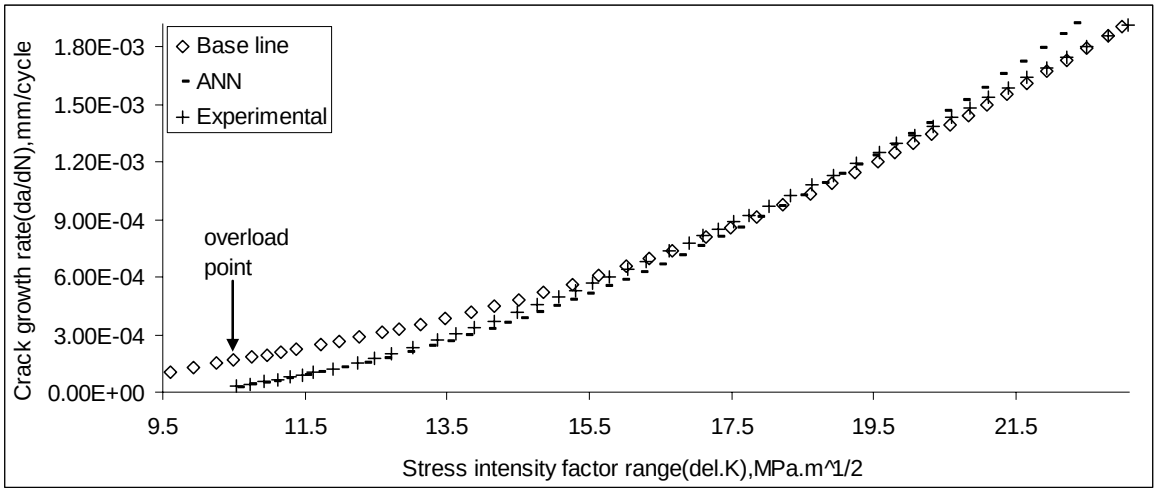

Fig. 8 - Comparison of predicted (ANN) and experimental crack growth rate (7020-T7)

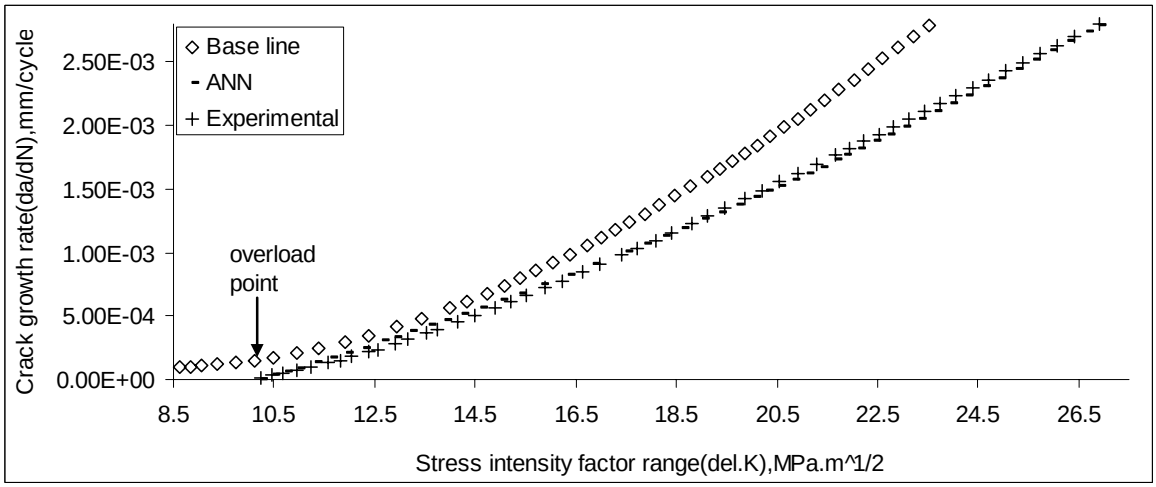

Fig. 9 - Comparison of predicted (ANN) and experimental crack growth rate (2024-T3)

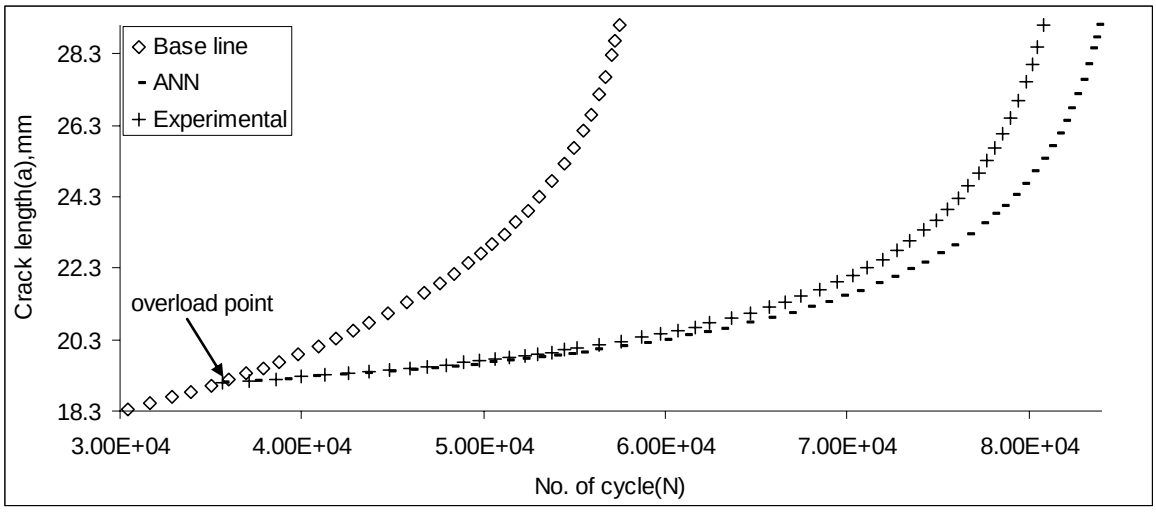

Fig. 10 - Comparison of predicted (ANN) and experimental number of cycle (7020-T7)

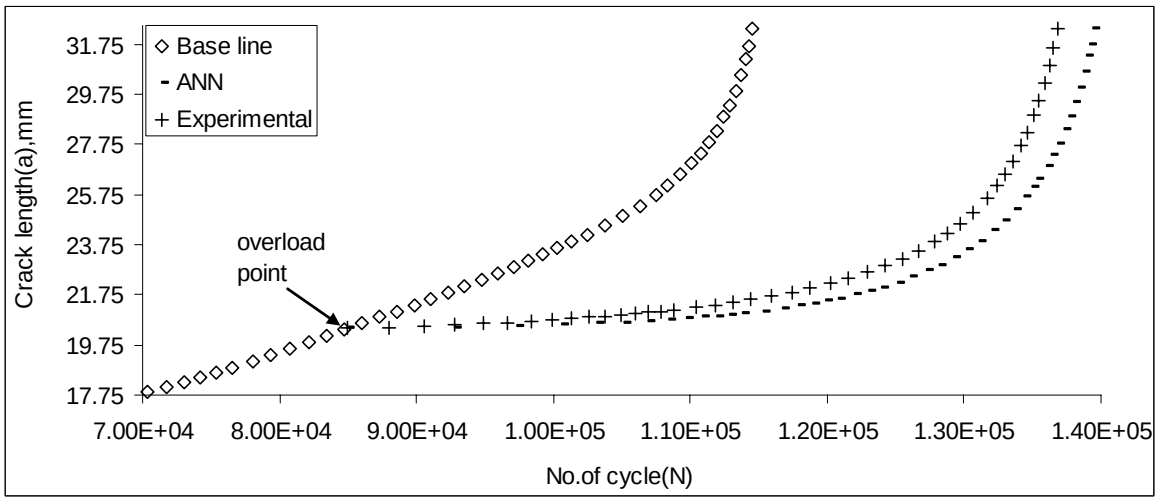

Fig. 11 - Comparison of predicted (ANN) and experimental number of cycle (2024-T3)

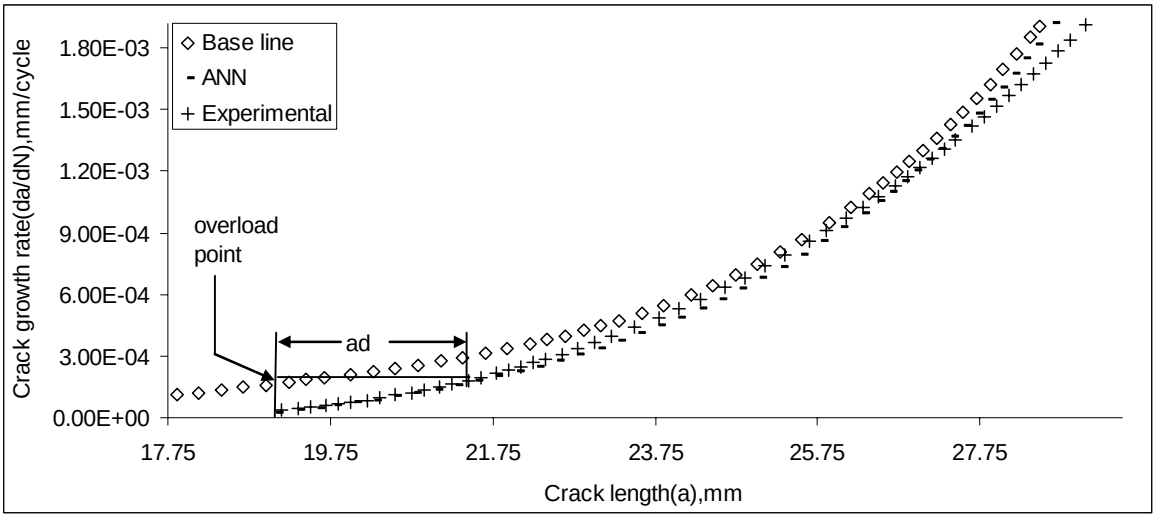

Fig. 12 - Comparison of predicted (ANN) and experimental crack growth rate with crack length (7020-T7)

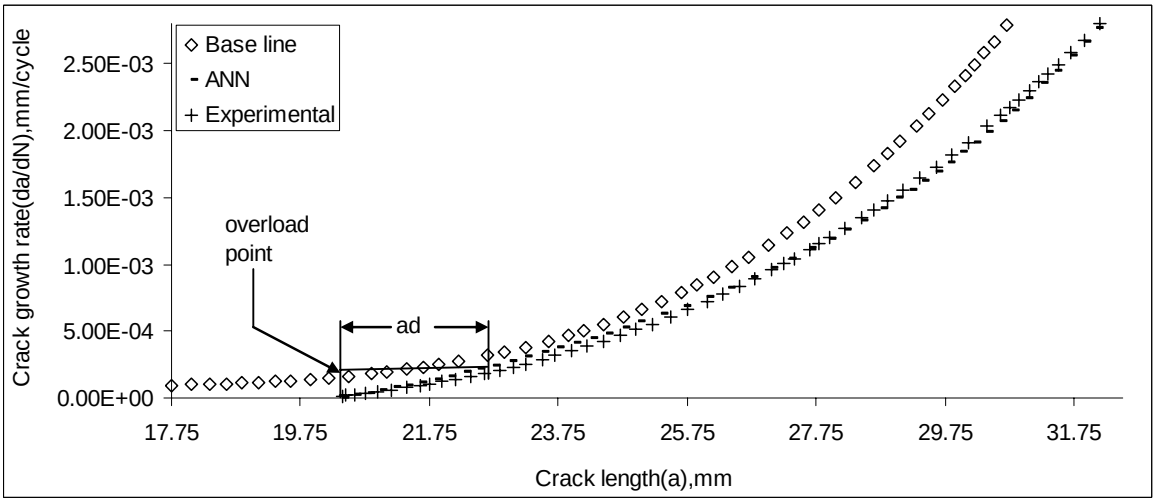

Fig. 13 - Comparison of predicted (ANN) and experimental crack growth rate with crack length (2024-T3)

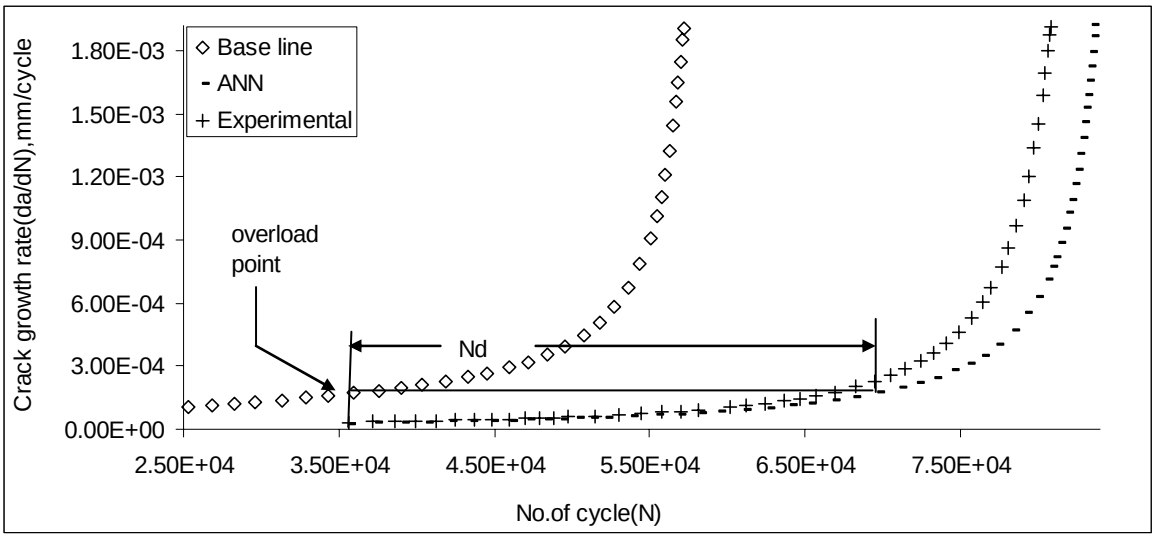

Fig. 14 - Comparison of predicted (ANN) and experimental crack growth rate with number of cycle (7020-T7)

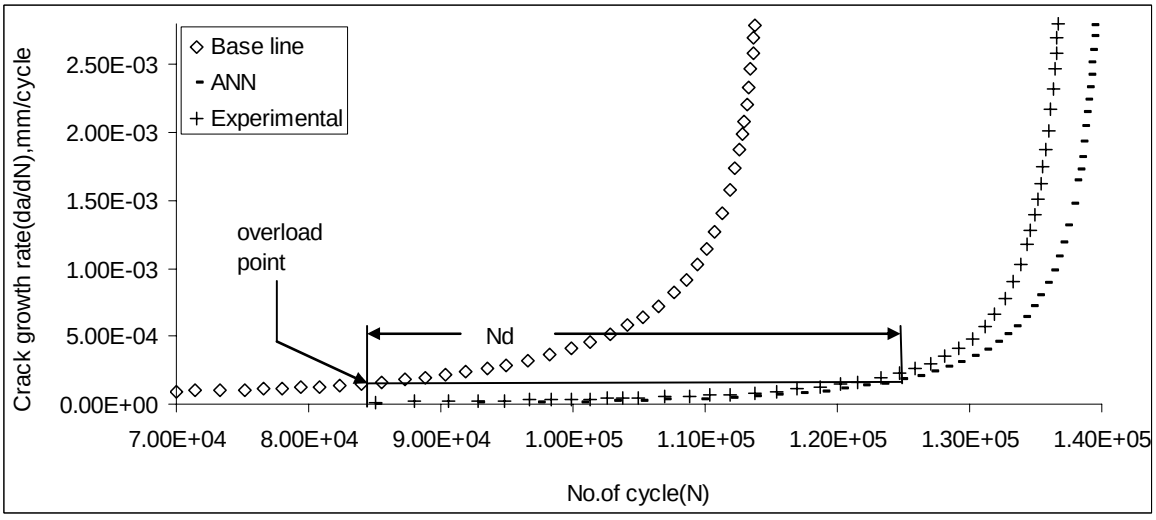

Fig. 15 - Comparison of predicted (ANN) and experimental crack growth rate with number of cycle (2024-T3)

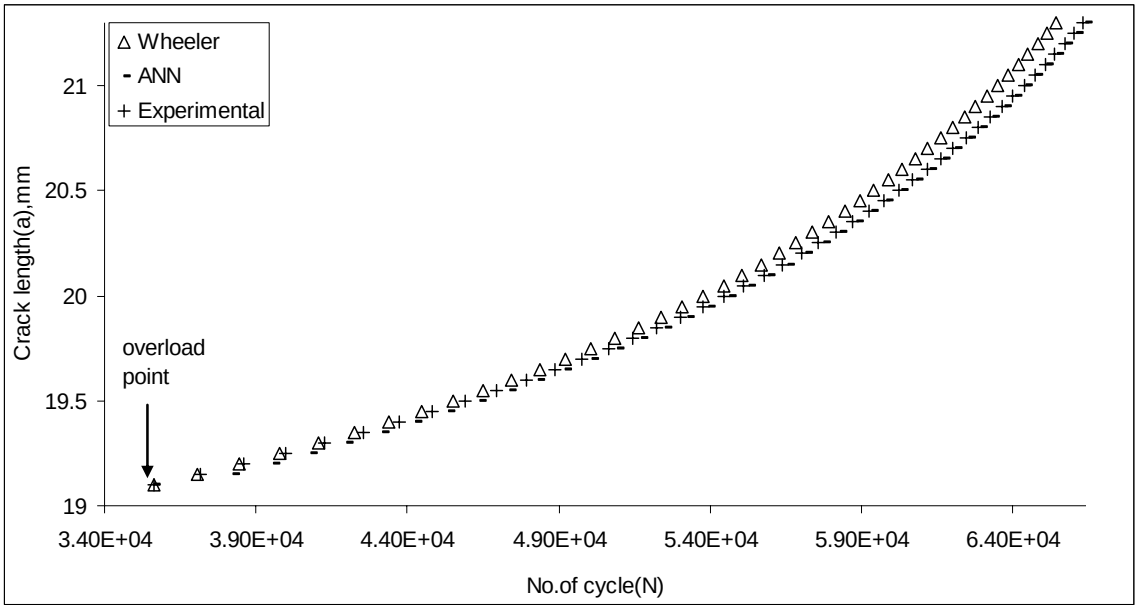

Fig. 16 - Comparison of Wheeler, predicted (ANN) and experimental number of cycle (7020-T7)

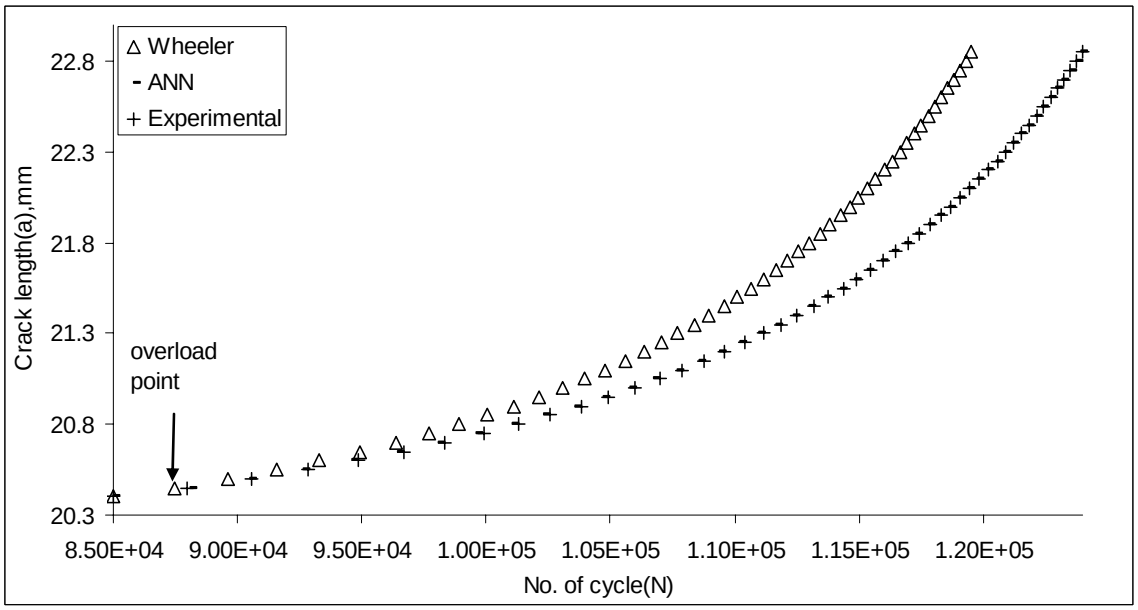

Fig. 17 - Comparison of Wheeler, predicted (ANN) and experimental number of cycle (2024-T3)

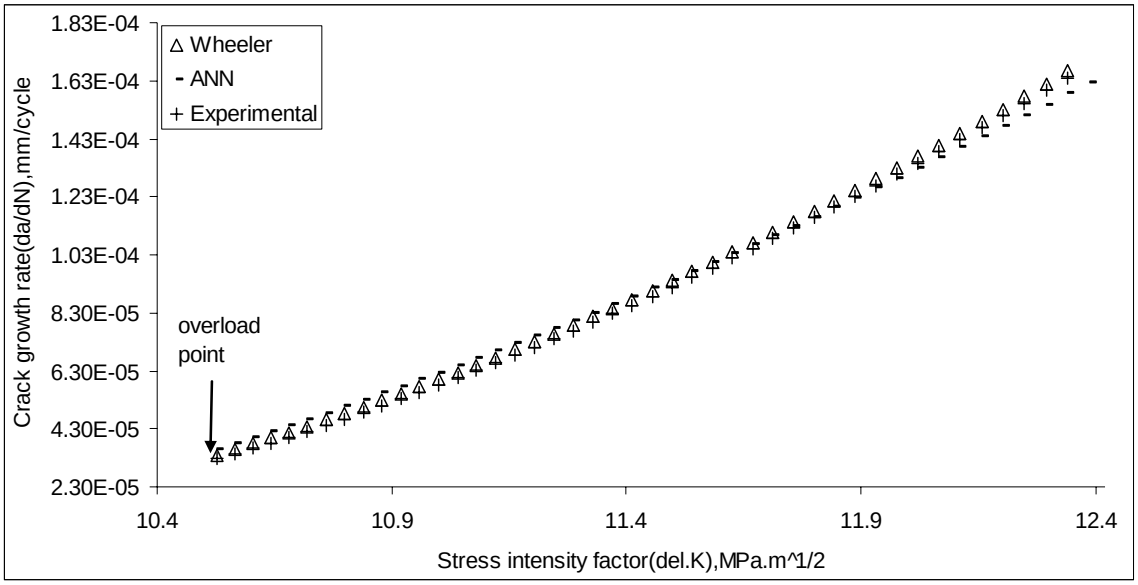

Fig. 18 - Comparison of Wheeler, predicted (ANN) and experimental crack growth rate (7020-T7)

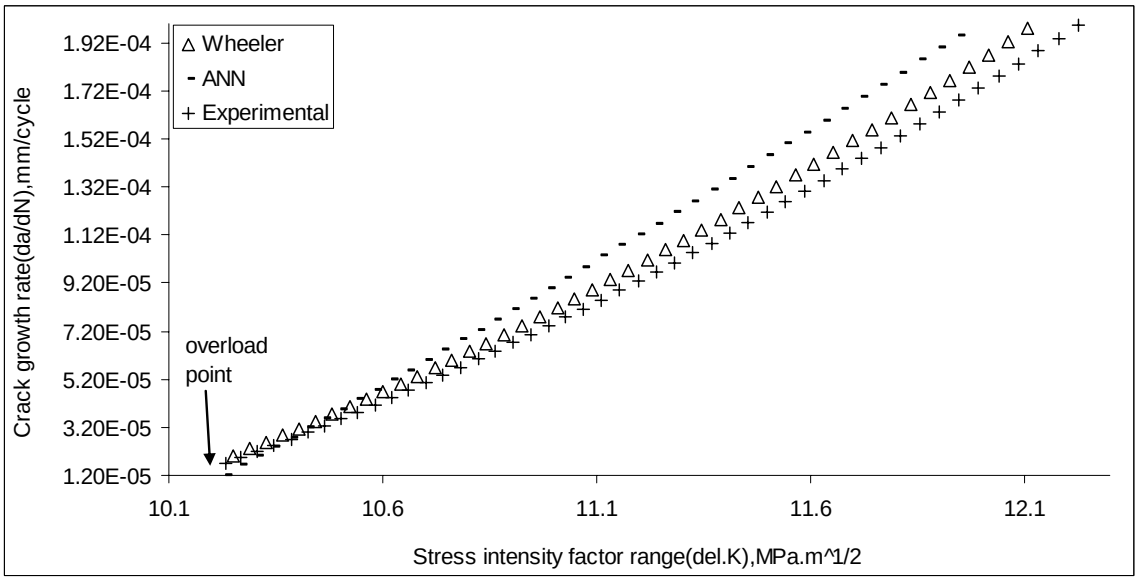

Fig. 19 - Comparison of Wheeler, predicted (ANN) and experimental crack growth rate (2024-T3)